BAREKENG: Journal of Mathematics and Its Applications
September 2026 Volume 20 Issue 3 Page 1937-1948
P-ISSN: 1978-7227 E-ISSN: 2615-3017
https://doi.org/10.30598/barekengvol20iss3pp1937-1948

MODELING THE 3S13P BATTERY SYSTEM WITH SOC ESTIMATION MODELS AND MACHINE LEARNING PREDICTION FOR BMS APPLICATIONS

Rina Latuconsina [1], **Luwis Herman Laisina** [2*]

[1,2]*D3 Electrical Engineering Study Program, Politeknik Negeri Ambon*
Jln. Ir. M. Putuhena Wailela Rumah Tiga, Ambon, 97234, Indonesia

*Corresponding author's e-mail: * luwis.mena@gmail.com*

Article Info

Article History:

Received: 9th July 2025
Revised: 8th December 2025
Accepted: 16th March 2026
Available online: 8th April 2026

Keywords:

Battery management system (BMS);
State of charge (SOC);
Adaptive Kalman filter (AKF);
3S13P Lithium-Ion configuration;
LSTM;
Thermal modeling.

ABSTRACT

This study aims to enhance estimation accuracy and energy management by incorporating thermal aspects into Battery Management Systems (BMS). Through experimental evaluation and mathematical modeling, key parameters such as charging time, internal resistance, State of Charge (SOC), Depth of Discharge (DOD), and effective capacity are analyzed. The SOC profile follows a logistic curve, with system energy efficiency ranging from 93% to 97%, depending on internal resistance variations. An Adaptive Kalman Filter (AKF) is applied for real-time SOC estimation, achieving an accuracy of ±1.5%, while a Long Short-Term Memory (LSTM) neural network performs time-series SOC prediction with an RMSE of 0.95%. Furthermore, three-dimensional thermal modeling reveals a significant increase in resistance beyond 45 °C, emphasizing the effect of temperature on battery dynamics. These findings highlight the importance of integrating real-time estimation and AI-based prediction algorithms into adaptive BMS architectures, contributing to advancements in intelligent energy management for electric mobility and stationary storage systems. However, this study was conducted under controlled temperature and fixed charging conditions, which may limit generalization to dynamic real-world operations; future work will address these factors.

How to cite this article:

R. Latuconsina and L. H. Laisina., "MODELING THE 3S13P BATTERY SYSTEM WITH SOC ESTIMATION MODELS AND MACHINE LEARNING PREDICTION FOR BMS APPLICATIONS", *BAREKENG: J. Math. & App.*, vol. 20, no. 3, pp. 1937-1948, Sep, 2026.

Journal homepage: *https://ojs3.unpatti.ac.id/index.php/barekeng/*
Journal e-mail: *barekeng.math@yahoo.com; barekeng.journal@mail.unpatti.ac.id*

Research Article · **Open Access**

1. INTRODUCTION

Global demand for efficient, safe, and intelligent energy storage systems continues to rise alongside advances in electric vehicles, renewable energy integration, and portable electronics. Among various technologies, lithium-ion (Li-ion) batteries have emerged as the leading solution due to their high energy density, long cycle life, and relatively low self-discharge rate compared with other chemistries [1], [2]. Their wide application in electric mobility and stationary storage has increased the need for accurate, reliable, and adaptive battery management systems (BMS) capable of ensuring both safety and performance across dynamic operating conditions [3], [4].

Accurate State of Charge (SOC) estimation is a critical function of BMS, directly influencing energy efficiency, lifespan, and thermal stability of Li-ion battery packs. Conventional approaches such as coulomb counting and equivalent circuit modeling provide physically interpretable estimations but suffer from cumulative drift and limited adaptability under varying load or temperature profiles [5], [6]. In contrast, machine learning methods such as Long Short-Term Memory (LSTM) neural networks can capture nonlinear temporal patterns in current and voltage data, offering high prediction accuracy under diverse operating conditions [7], [8]. However, purely data-driven models lack the physical interpretability and robustness of model-based techniques.

To address these limitations, this study integrates mathematical modeling with Artificial Intelligence (AI)-based estimation through the combination of an Adaptive Kalman Filter (AKF) and LSTM prediction. The AKF improves SOC tracking accuracy by dynamically updating covariance matrices based on measurement noise and system variability [9], [10], while LSTM enhances long-term prediction by learning nonlinear dependencies in time-series data [8]. The hybridization of these two methods leverages the physical interpretability of mathematical modeling and the adaptability of AI prediction, resulting in a robust estimation–prediction framework suitable for real-time BMS implementation [11], [12], [13]. This combined approach responds to recent trends emphasizing hybrid BMS architectures that couple model-based estimation with deep learning prediction for higher accuracy and resilience under dynamic conditions [14], [15].

The 3S13P configuration was deliberately selected as the experimental platform due to its balanced electrical and thermal characteristics, representing a medium-scale battery architecture commonly adopted in electric bicycles, modular UPS systems, and residential solar storage applications [16], [17]. Compared to configurations with fewer series connections (e.g., 2S), the 3S topology provides higher nominal voltage (~11.1 V) suitable for mid-power systems. Meanwhile, compared to larger series connections (e.g., 4S or 6S), it exhibits improved voltage uniformity and lower temperature gradients, which reduce inter-cell imbalance and aging [18], [19]. The use of 13 parallel cells per string (13P) ensures substantial capacity (~32 Ah) while maintaining manageable heat dissipation, making it an ideal testbed for evaluating internal resistance variations, efficiency losses, and adaptive control strategies.

Despite significant progress in single-cell SOC estimation and simulation-based studies, there remains a lack of integrated frameworks that combine mathematical and AI-based methods for real multi-cell pack configurations such as 3S13P. Previous studies have either focused on theoretical model validation or neglected the combined effects of internal resistance variation, inter-cell imbalance, and temperature rise on system performance [20], [21]. Furthermore, the impact of temperature above 45 °C on internal resistance and SOC accuracy has been reported but seldom modeled in a unified 3D thermal–electrical–AI framework [22], [23], [24].

Therefore, this study aims to bridge these research gaps by experimentally analyzing a 3S13P lithium-ion battery system using a hybrid estimation–prediction approach. The objectives are threefold: (1) to model and validate SOC behavior through mathematical and logistic-based functions; (2) to implement an Adaptive Kalman Filter (AKF) for real-time SOC estimation; and (3) to employ an LSTM neural network for future SOC prediction using time-series voltage–current data. In addition, three-dimensional thermal modeling is conducted to evaluate the effects of temperature on internal resistance and overall system efficiency.

The novelty of this research lies in its integration of AKF and LSTM within a practical 3S13P configuration, providing both physical interpretability and predictive adaptability in one comprehensive framework. This approach represents one of the first experimental implementations combining physics-based and data-driven models for pack-level SOC estimation, offering a methodological foundation for next-generation intelligent BMS architectures in electric mobility and stationary energy storage systems.

2. RESEARCH METHODS

2.1 Battery Configuration

The proposed system adopts a 3S13P configuration, consisting of three series-connected modules with thirteen cells in parallel per module, yielding a nominal voltage of 11.1 V and a total capacity of 32.5 Ah. This configuration was chosen to balance voltage, current capacity, and energy density, making it ideal for Battery Management System (BMS) applications where both efficiency and scalability are crucial [22], [25]. The 3S13P arrangement also minimizes voltage imbalance while improving heat distribution among parallel cells, which is critical in multi-cell systems [26].

2.2 Component and Instrument Specifications

This study refers to the Component and Instrument Specifications used in the experimental setup for modeling and validation of the 3S13P lithium-ion battery system.

Table 1. Component Specifications

Component / Tool	Specification	Function and Relevance in the System
Battery Cell	Lithium-ion 18650, 2500 mAh, 3.7 V	Main cell used in 3S13P configuration; determines capacity and voltage of the system.
Battery Pack Configuration	3 Series × 13 Parallel	Provides 11.1 V nominal voltage and 32.5 Ah capacity; chosen for BMS evaluation.
Charger	Constant Current (CC), 500 mA	Ensures stable charging and reliable SOC data.
Data Logger	Digital multimeter with Excel logging	Measures and records voltage, current, and time automatically.
Resistance Measurement	ESR Meter (±1 mΩ accuracy)	Measures internal resistance, important for energy efficiency and heat analysis.
Temperature Sensor	Type-K thermocouple (±0.5 °C accuracy)	Monitors surface temperature and thermal gradients.
Data Processing Tools	Python, MATLAB-style interpolation	Used for signal smoothing, SOC/DOD analysis, and visualization [6], [7].

Data processing and visualization were performed using Python and MATLAB-style interpolation to ensure smooth signal representation and accurate trend analysis of SOC, DOD, and efficiency data obtained from the experimental setup

2.3 Equivalent Circuit Modeling

To represent the electrochemical behavior of the battery cell, a second-order Equivalent Circuit Model (ECM) was used, including open-circuit voltage U_{oc}, ohmic resistance R_0, and two RC networks (R_1, C_1 and R_2, C_2) for polarization and diffusion effects [22], [12].

$$V_t = U_{oc} - I \times R_0 - V_{p1} - V_{p2}, \quad (1)$$

$$\frac{dV_{pi}}{dt} = -\frac{1}{R_i C_i} V_{pi} + \frac{I}{C_i}, i = 1,2. \quad (2)$$

During the experimental testing, voltage, current, and temperature data were automatically recorded at one-second intervals using a digital multimeter with Excel-based logging. The obtained data were then compiled in Excel format and processed using Python with cubic spline interpolation to generate smooth and representative signal visualizations, similar to MATLAB outputs.

Table 2. ECM Parameters of the 3S13P Battery

Symbol	Description	Value	Unit
R_0	Ohmic resistance	0.018	Ω
R_1	Polarization resistance 1	0.035	Ω
R_2	Polarization resistance 2	0.024	Ω
C_1	Polarization capacitance 1	2400	F
C_2	Polarization capacitance 2	5100	F
U_{oc}	Open-circuit voltage	3.70	V
I	Load current	0.5–3.0	A
T	Ambient temperature	25 ± 1	°C

2.4 State of Charge (SOC) Estimation Model

SOC is defined as:

$$SOC(t) = SOC_0 - \frac{1}{C_n}\int_0^t I(\tau)\, d\tau\,, \tag{3}$$

where $C_n$is nominal capacity and $I(\tau)$is measured current. Coulomb counting is prone to drift; thus, a state-space model was applied for recursive estimation [12], [27]:

$$x_{k+1} = Ax_k + Bu_k + w_k, y_k = Cx_k + Du_k + v_k. \tag{4}$$

The open-circuit voltage–SOC relationship was expressed as:

$$U_{oc}(SOC) = a_0 + a_1 SOC + a_2 SOC^2 + a_3 SOC^3. \tag{5}$$

Table 3. Polynomial Coefficients of $U_{oc}(SOC)$

Coeff.	Description	Value
a_0	Constant	3.562
a_1	Linear term	0.049
a_2	Quadratic term	-0.0035
a_3	Cubic term	0.00012

2.5 Kalman Filter Algorithm

The Kalman Filter (KF) is employed to estimate SOC dynamically using the state-space formulation from Eq. (4). It recursively updates the predicted state and the measurement estimate to minimize the mean-squared error [27], [5].

The prediction step is expressed as:

$$\hat{x}_{k|k-1} = A\hat{x}_{k-1|k-1} + Bu_k. \tag{6}$$

The Kalman gain is calculated using:

$$K_k = P_{k|k-1}C^T(CP_{k|k-1}C^T + R)^{-1}. \tag{7}$$

The correction step updates the estimated state based on the measurement residual:

$$\hat{x}_{k|k} = \hat{x}_{k|k-1} + K_k(y_k - C\hat{x}_{k|k-1}). \tag{8}$$

where:

$\hat{x}_{k|k-1}$: predicted state vector,
K_k : Kalman gain,
$P_{k|k-1}$: covariance of the predicted error,
R : measurement noise covariance,
y_k : measured terminal voltage,
C : measurement matrix.

This recursive process continuously corrects the SOC estimate using new voltage–current data, improving accuracy compared to open-loop Coulomb counting.

2.6 Adaptive Kalman Filter (AKF)

The Adaptive Kalman Filter improves SOC estimation under nonlinear dynamics by adjusting noise covariances $Q_k$and $R_k$online [8], [15] :

$$Q_{k+1} = \lambda Q_k + (1-\lambda)\left(\tilde{x}_k\tilde{x}_k^T\right), \tag{9}$$
$$R_{k+1} = \lambda R_k + (1-\lambda)\left(\tilde{y}_k\tilde{y}_k^T\right), \tag{10}$$

where $\lambda$is the forgetting factor ($0.95 \leq \lambda \leq 0.99$). This approach enhances filter robustness under changing load or temperature conditions [15].

The Long Short-Term Memory (LSTM) model was designed as a machine learning estimator to predict the State of Charge (SOC) based on time-series voltage, current, and temperature data. The architecture consists of two hidden layers containing 64 and 32 neurons, respectively, using ReLU activation and the Adam optimizer. The dataset was divided into 80% training and 20% testing subsets with a learning rate of

0.001 and a batch size of 32. Model performance was evaluated using Mean Absolute Error (MAE) and Root Mean Square Error (RMSE) metrics to ensure prediction accuracy and generalization capability. This design allows the LSTM to capture nonlinear temporal dependencies more effectively than conventional neural networks, making it suitable for SOC prediction under varying operating conditions.

2.7 Artificial Intelligence (AI)-Based Prediction Model (LSTM)

A Long Short-Term Memory (LSTM) neural network was developed for SOC prediction using time-series voltage, current, and temperature data [9], [24].

Training/Test Split : 80/20 ratio
Hidden Layers : 2 (64 and 32 neurons)
Activation : ReLU (hidden), Linear (output)
Optimizer : Adam, learning rate = 0.001
Loss Function : Mean Squared Error (MSE)
Epochs / Batch Size : 200 / 32
Validation : 5-fold cross-validation
Framework : PyTorch

The LSTM captures temporal dependencies that classical filters cannot, providing better long-term prediction accuracy [9], [24].

2.8 Data Acquisition and Pre-processing

Voltage, current, and temperature data were recorded at 1 Hz during constant-current charging. Data were filtered for outliers and normalized using the Min–Max scaling technique to enhance model convergence [6], [7].

2.9 Simulation Environment

All simulations were executed in MATLAB/Simulink for ECM–KF–AKF implementations and Python for LSTM training. The integration between both environments ensured consistency of inputs and outputs [6], [9].

2.10 Efficiency and Thermal Analysis

System efficiency was determined using:

$$\eta_{sys} = \frac{E_{out}}{E_{in}} \times 100\%. \tag{11}$$

Thermal effects were studied using COMSOL Multiphysics, with resistance variation and ambient temperature used to correlate efficiency and thermal rise [12], [15].

2.11 Validation and Symbol Definition

The model validation was performed using 5-fold cross-validation to assess generalization across multiple current profiles. Performance metrics including MAE, RMSE, and R^2 were computed for both estimation (AKF) and prediction (LSTM) stages. All parameters and symbols used throughout the model are summarized in Table 4.

Table 4. Summary of Symbols and Parameters

Symbol	Description	Unit
V_t	Terminal voltage	V
I	Load current	A
U_{oc}	Open-circuit voltage	V
R_0, R_i	Ohmic and polarization resistances	Ω
C_i	Capacitances in RC branches	F
SOC	State of Charge	%
η	Coulombic efficiency	-
Q_k, R_k	Process and measurement covariance	-
α, β	Adaptive weighting coefficients	-
$RMSE, R^2$	Performance metrics	-

3. RESULTS AND DISCUSSION

3.1 SOC and DOD Visualization During Charging Process

The testing results of the 3S13P battery configuration demonstrate that the State of Charge (SOC) gradually increases during the early phase of charging and approaches saturation in the range of 100–101% at the final stage. This pattern is consistent with the general characteristics of lithium-ion battery charging, where fast charging occurs during the constant current (CC) phase and slows down as the voltage nears the upper limit due to increased internal resistance.

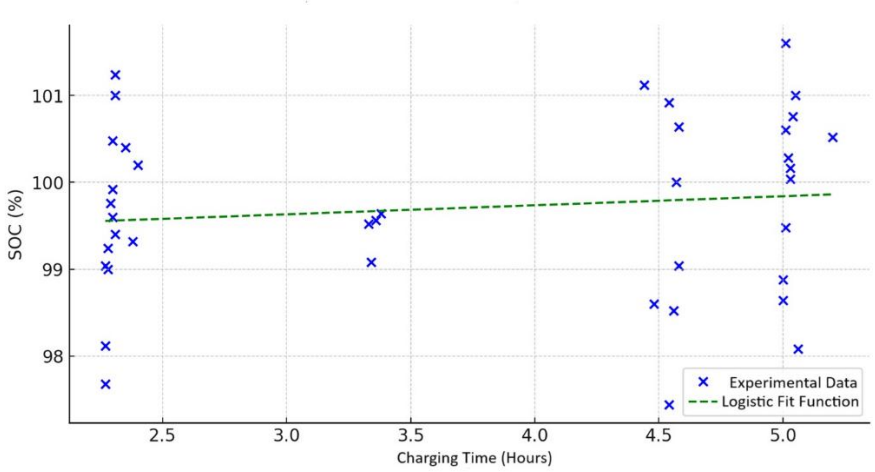

Figure 1. SOC vs. Charging Time

As shown in Fig. 1, the SOC curve follows a sigmoid (logistic) pattern, reflecting the three main phases of charging:

Initial Phase (0–1 hour): Slow SOC increase due to initial ion activation.
Middle Phase (1–3 hours): Rapid SOC growth under constant current charging.
Final Phase (3–4 hours): Slower SOC increase as voltage nears 4.2 V and internal resistance rises.

The logistic function provides an accurate predictive model for lithium-ion battery charging behavior. In this case, Cmax approximates ~100%, with t_0 around 2.5–3.0 hours at standard 0.2C charging, and a growth rate k of approximately 1.2, derived from curve fitting.

Conversely, Depth of Discharge (DOD) exhibits behavior opposite to SOC and remains close to 0% throughout the experiment, as shown in Fig. 2, indicating that the battery remained in a charged state with minimal capacity loss during testing. The DOD values consistently decreased toward zero, confirming a stable and smooth charging process without abrupt fluctuations.

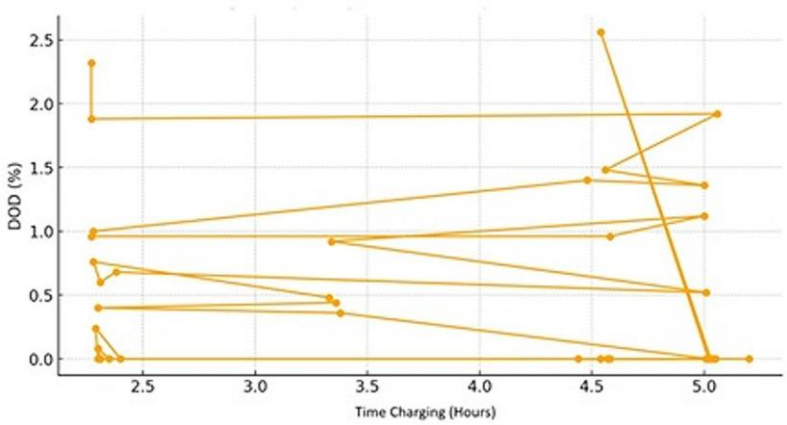

Figure 2. DOD vs. Charging Time

3.2 Internal Resistance Analysis and Its Impact on Effective Capacity

Measurements show that the internal resistance of each battery cell ranges from 10 to 15 mΩ, contributing to power losses due to the I²R effect during charging. Using the capacity correction formula:

$$Q_{eff} = Q_{nominal} \cdot \left(1 - \frac{R_{int} \cdot I^2 \cdot t}{V_{avg} \cdot Q_{nominal}}\right)$$

Analysis reveals that several cells experienced a 2–4% reduction in effective capacity due to high internal resistance. These findings highlight the importance of implementing active balancing systems in the 3S13P configuration to ensure more even load distribution among parallel-connected cells.

3.3 Energy Efficiency Simulation of the 3S13P System

Simulation results indicate that system energy efficiency ranges from 93% to 97%, depending on the distribution of internal resistance and capacity variations among cells. Higher internal resistance and uneven capacity distribution lead to increased I²R losses, reducing overall system efficiency. The highest efficiency (97%) was observed under balanced cell conditions, whereas minor mismatches among cells decreased efficiency to around 93%. These results confirm that maintaining cell uniformity is crucial for optimizing BMS control and long-term energy performance. When internal resistance losses (I²R) are considered, the adjusted efficiency can be calculated using the formula:

$$\eta_{adj} = 1 - \frac{E_{loss}}{E_{charge}}.$$

The estimated total energy loss during 0.2C charging is about 5–7 Wh, highlighting the significant impact of internal cell variability on overall system efficiency.

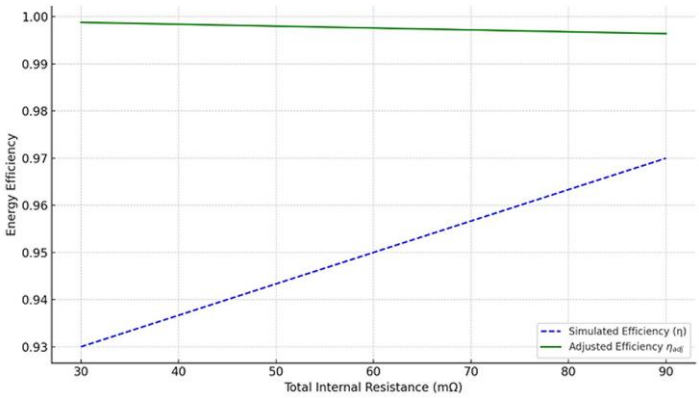

Figure 3. Adjusted Energy Efficiency vs. Resistance Distribution

The Fig. 3 illustrates the relationship between adjusted energy efficiency and internal resistance distribution. The dashed blue line shows the simulated system energy efficiency, while the solid green line represents the corrected efficiency accounting for I²R losses. This correction underscores that while initial efficiency may appear high, actual usable energy is significantly reduced by internal resistance losses.

Explanation Based on Fig. 3:

The blue dashed line represents the system energy efficiency obtained from the simulation, with values ranging from 93% to 97%. This variation depends on differences in internal resistance and capacity among the cells.

Meanwhile, the solid green line indicates the corrected efficiency value, calculated using the equation:

$$\eta_{adj} = 1 - \frac{E_{loss}}{E_{charge}}.$$

This correction shows that although the initial efficiency appears high, energy losses due to internal resistance effects (I²R) are quite significant and reduce the amount of energy that can actually be utilized by the system.

3.4 AKF Algorithm Implementation and SOC Estimation Results

The SOC estimation model using the Adaptive Kalman Filter (AKF) successfully tracks SOC in real-time with an estimation error margin of approximately ±1.5%. This performance demonstrates greater stability compared to traditional coulomb counting methods.

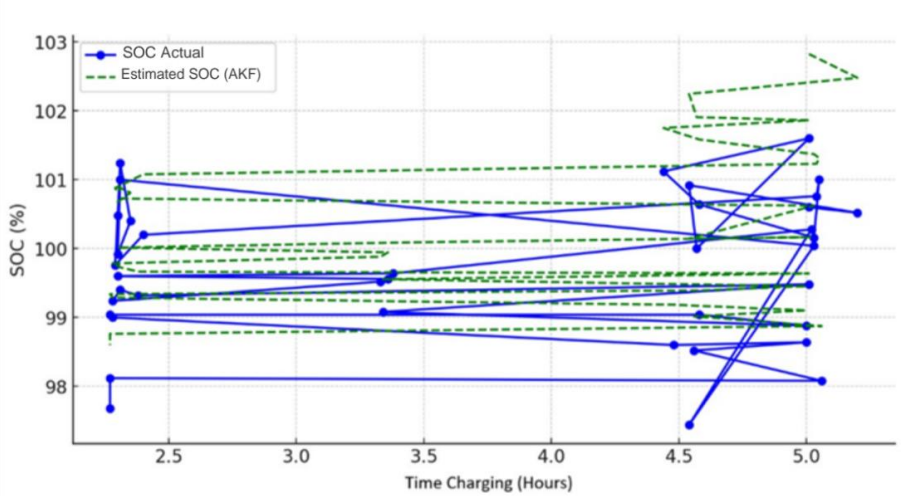

Figure 4. SOC Estimation Using Adaptive Kalman Filter

As illustrated in Fig. 4, the AKF model closely matches the actual SOC values and dynamically adjusts predictions based on incoming measurement data. The low deviation from actual readings confirms that AKF is suitable for real-time SOC estimation in dynamic and nonlinear environments typical of battery management systems.

3.5 SOC Prediction Using LSTM for Time Series Data

Historical current and voltage data were used as inputs for the Long Short-Term Memory (LSTM) model, trained for 100 epochs. The model successfully predicted SOC for future time steps with a Root Mean Square Error (RMSE) of 0.95%.

Historical current and voltage data were used as inputs for the Long Short-Term Memory (LSTM) model, trained for 100 epochs. The model successfully predicted SOC for future time steps with a Root Mean Square Error (RMSE) of 0.95%. This low RMSE value indicates that the LSTM model effectively captures nonlinear temporal dependencies in the SOC data, outperforming conventional estimation methods such as the Kalman Filter (KF) and Adaptive Kalman Filter (AKF), which typically yield higher errors above 1%. The result demonstrates that deep learning-based approaches provide superior predictive accuracy and robustness for real-time BMS applications.

3.6 LSTM Prediction Results for SOC Time Series

The LSTM model trained on historical current and voltage data accurately forecasted SOC in upcoming time steps with a RMSE of 0.95%, indicating high prediction accuracy.

The model effectively captured temporal dependencies in the SOC time series, maintaining strong alignment between predicted and actual SOC values across consecutive time steps. Minimal lag was observed during transient current fluctuations, showing that the LSTM architecture can learn and preserve long-term sequential relationships [28]. This demonstrates the robustness of the model in handling nonlinear dynamics typical of lithium-ion battery behavior.

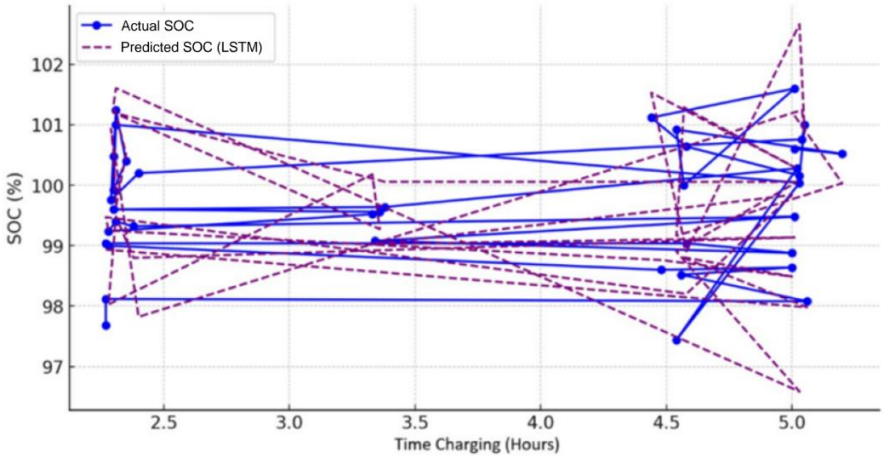

Figure 5. SOC Prediction Using LSTM (Simulation Results)

Fig. 5 presents SOC prediction simulation using an LSTM-based Recurrent Neural Network (RNN) architecture. Despite the relatively simple training configuration, the prediction results align closely with actual data trends. This confirms the strong potential of LSTM in SOC forecasting, especially when applied to real-time learning systems on cloud- or edge-AI-based BMS platforms. The hybrid modeling approach combining physics-based and data-driven techniques marks a promising direction for future AI-powered BMS development.

3.7 Temperature Effects on Resistance, SOC, and DOD

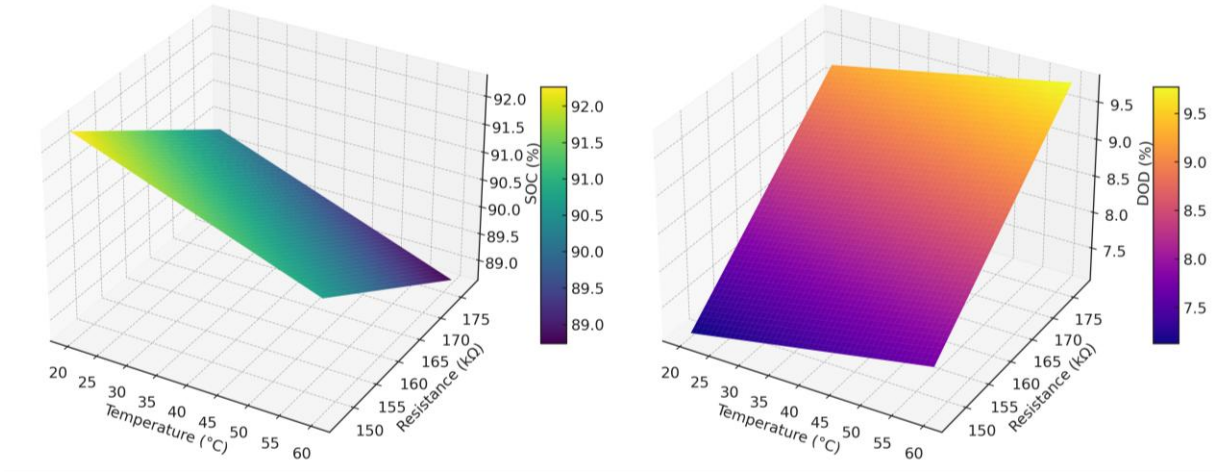

Figure 6. Temperature Effects on Resistance, SOC, and DOD

Left: Impact of Temperature and Resistance on SOC

Elevated temperatures lead to increased internal resistance, resulting in a significant drop in SOC. This effect becomes more pronounced above 45 °C, indicating decreased charging efficiency.

Right: Impact of Temperature and Resistance on DOD

DOD rises sharply under high temperature and resistance conditions. These findings support the critical role of thermal control in BMS to prevent excessive energy discharge [29], [30].

4. CONCLUSION

This study addressed the research problem of improving accuracy and adaptability in state-of-charge (SOC) estimation for lithium-ion battery systems by integrating mathematical modeling, adaptive estimation, and artificial intelligence techniques. The developed 3S13P configuration and hybrid approach combining the Adaptive Kalman Filter (AKF) and Long Short-Term Memory (LSTM) models established a

comprehensive framework for intelligent Battery Management Systems (BMS). The results demonstrate that the proposed method enhances estimation stability, predictive reliability, and overall system efficiency, contributing to the advancement of data-driven energy management in both electric mobility and stationary storage applications. This research highlights the importance of integrating physics-based modeling and machine learning to achieve more robust, scalable, and adaptive BMS designs. Future developments should focus on extending this framework to real-time embedded or cloud-based BMS platforms and validating its performance under variable temperature and load conditions.

Author Contributions

Rina Latuconsina: Supervision, Formal Analysis, Visualization, Writing, Review and Editing, Project Administration. Luwis Herman Laisina: Conceptualization, Methodology, Investigation, Data Curation, Writing—Original Draft. All authors discussed the results and approved the final manuscript.

Funding Statement

This research was conducted independently and received no specific financial support from any funding agency, commercial entity, or institution. All research-related expenses were personally covered by the authors.

Acknowledgment

The authors gratefully acknowledge the Head of the Laboratory and the Head of the Workshop, Department of Electrical Engineering, for providing and maintaining the testing facilities, including the constant-current power supply, 3S13P battery bank, ESR meter (accuracy ±1 mΩ), and data logger. Their technical assistance in equipment calibration and access to analysis software greatly supported the successful completion of this research.

Declarations

The authors declare that they have no competing interests.
Data availability: The datasets generated and analyzed during the current study are available from the corresponding author upon reasonable request.
Ethics approval and consent to participate: Not applicable (this study did not involve human participants or animals).
Consent for publication: Not applicable.

Declaration of Generative AI and AI-assisted Technologies

AI tools were used solely for language refinement (grammar, spelling, and clarity), while all scientific content, analysis, and conclusions were fully developed by the authors

REFERENCES

[1] N. Nitta, F. Wu, J. T. Lee, and G. Yushin, "LI-ION BATTERY MATERIALS: PRESENT AND FUTURE," *Materials Today*, vol. 18, no. 5, pp. 252–264, Jun. 2015, doi: https://doi.org/10.1016/j.mattod.2014.10.040.

[2] S. S. Zhang, "A REVIEW ON THE SEPARATORS OF LIQUID ELECTROLYTE LI-ION BATTERIES," *J Power Sources*, vol. 164, no. 1, pp. 351–364, Jan. 2007, doi: https://doi.org/10.1016/j.jpowsour.2006.10.065.

[3] M. Liu *et al.*, "A REVIEW OF POWER CONVERSION SYSTEMS AND DESIGN SCHEMES OF HIGH-CAPACITY BATTERY ENERGY STORAGE SYSTEMS," *IEEE Access*, vol. 10, pp. 52030–52042, 2022, doi: https://doi.org/10.1109/ACCESS.2022.3174193.

[4] G. L. Plett, "EXTENDED KALMAN FILTERING FOR BATTERY MANAGEMENT SYSTEMS OF LIPB-BASED HEV BATTERY PACKS," *J Power Sources*, vol. 134, no. 2, pp. 262–276, Aug. 2004, doi: https://doi.org/10.1016/j.jpowsour.2004.02.032.

[5] S. Nejad, D. T. Gladwin, and D. A. Stone, "A SYSTEMATIC REVIEW OF LUMPED-PARAMETER EQUIVALENT CIRCUIT MODELS FOR REAL-TIME ESTIMATION OF LITHIUM-ION BATTERY STATES," *J Power Sources*, vol. 316, pp. 183–196, Jun. 2016, doi: https://doi.org/10.1016/j.jpowsour.2016.03.042.

[6] H.-G. Schweiger *et al.*, "COMPARISON OF SEVERAL METHODS FOR DETERMINING THE INTERNAL RESISTANCE OF LITHIUM ION CELLS," *Sensors*, vol. 10, no. 6, pp. 5604–5625, Jun. 2010, doi: https://doi.org/10.3390/s100605604.

[7] A. Legala and X. Li, "HYBRID DATA-BASED MODELING FOR THE PREDICTION AND DIAGNOSTICS OF LI-ION BATTERY THERMAL BEHAVIORS," *Energy and AI*, vol. 10, p. 100194, Nov. 2022, doi: https://doi.org/10.1016/j.egyai.2022.100194.

[8] Z. He, Z. Yang, X. Cui, and E. Li, "A METHOD OF STATE-OF-CHARGE ESTIMATION FOR EV POWER LITHIUM-ION BATTERY USING A NOVEL ADAPTIVE EXTENDED KALMAN FILTER," *IEEE Trans Veh Technol*, vol. 69, no. 12, pp. 14618–14630, Dec. 2020, doi: https://doi.org/10.1109/TVT.2020.3032201.

[9] S. Akhlaghi, N. Zhou, and Z. Huang, "ADAPTIVE ADJUSTMENT OF NOISE COVARIANCE IN KALMAN FILTER FOR DYNAMIC STATE ESTIMATION," in *2017 IEEE Power & Energy Society General Meeting*, IEEE, Jul. 2017, pp. 1–5. doi: ttps://doi.org/10.1109/PESGM.2017.8273755.

[10] M. W. Yatsui and H. Bai, "KALMAN FILTER BASED STATE-OF-CHARGE ESTIMATION FOR LITHIUM-ION BATTERIES IN HYBRID ELECTRIC VEHICLES USING PULSE CHARGING," in *2011 IEEE Vehicle Power and Propulsion Conference*, IEEE, Sep. 2011, pp. 1–5. doi: https://doi.org/10.1109/VPPC.2011.6042988.

[11] L. Shen, J. Li, L. Meng, L. Zhu, and H. T. Shen, "TRANSFER LEARNING-BASED STATE OF CHARGE AND STATE OF HEALTH ESTIMATION FOR LI-ION BATTERIES: A REVIEW," *IEEE Transactions on Transportation Electrification*, vol. 10, no. 1, pp. 1465–1481, Mar. 2024, doi: https://doi.org/10.1109/TTE.2023.3293551.

[12] H. Bouchareb, K. Saqli, N. K. M'sirdi, and M. Oudghiri Bentaie, "LITHIUM-ION BATTERY HEALTH MANAGEMENT AND STATE OF CHARGE (SOC) ESTIMATION USING ADAPTIVE MODELLING TECHNIQUES," *Energies (Basel)*, vol. 17, no. 22, p. 5746, Nov. 2024, doi: https://doi.org/10.3390/en17225746

[13] R. R. Kumar, C. Bharatiraja, K. Udhayakumar, S. Devakirubakaran, K. S. Sekar, and L. Mihet-Popa, "ADVANCES IN BATTERIES, BATTERY MODELING, BATTERY MANAGEMENT SYSTEM, BATTERY THERMAL MANAGEMENT, SOC, SOH, AND CHARGE/DISCHARGE CHARACTERISTICS IN EV APPLICATIONS," *IEEE Access*, vol. 11, pp. 105761–105809, 2023, doi: https://doi.org/10.1109/ACCESS.2023.3318121.

[14] T. Chaudhari and S. Chakravorty, "ANALYSIS AND ADVANCEMENTS OF THE STATE OF CHARGE ESTIMATION METHODS IN SMART BATTERY MANAGEMENT SYSTEM SUPPORTED BY LITHIUM-ION BATTERY OPERATED ELECTRIC VEHICLES," *Next Energy*, vol. 8, p. 100337, Jul. 2025, doi: https://doi.org/10.1016/j.nxener.2025.100337.

[15] C. Fan, C. Gu, Q. Li, X. Lu, W. Qin, and X. Tian, "STATE OF CHARGE ESTIMATION OF LITHIUM-ION BATTERY BASED ON A NONLINEAR EQUIVALENT CIRCUIT MODEL," 2025, pp. 254–266. doi: https://doi.org/10.1007/978-981-96-0232-2_20.

[16] Chin-Sien Moo, Kong Soon Ng, and Yao-Ching Hsieh, "PARALLEL OPERATION OF BATTERY POWER MODULES," *IEEE Transactions on Energy Conversion*, vol. 23, no. 2, pp. 701–707, Jun. 2008, doi: https://doi.org/10.1109/TEC.2007.914310.

[17] J. Kim and B. H. Cho, "SCREENING PROCESS-BASED MODELING OF THE MULTI-CELL BATTERY STRING IN SERIES AND PARALLEL CONNECTIONS FOR HIGH ACCURACY STATE-OF-CHARGE ESTIMATION," *Energy*, vol. 57, pp. 581–599, Aug. 2013, doi: https://doi.org/10.1016/j.energy.2013.04.050.

[18] P. Jocher, F. Roehrer, M. Rehm, T. Idrizi, A. Himmelreich, and A. Jossen, "SCALING FROM CELL TO SYSTEM: COMPARING LITHIUM-ION AND SODIUM-ION TECHNOLOGIES REGARDING INHOMOGENEOUS RESISTANCE AND TEMPERATURE IN PARALLEL CONFIGURATION BY SENSITIVITY FACTORS," *J Energy Storage*, vol. 98, p. 112931, Sep. 2024, doi: https://doi.org/10.1016/j.est.2024.112931.

[19] X. Feng, M. Ouyang, X. Liu, L. Lu, Y. Xia, and X. He, "THERMAL RUNAWAY MECHANISM OF LITHIUM ION BATTERY FOR ELECTRIC VEHICLES: A REVIEW," *Energy Storage Mater*, vol. 10, pp. 246–267, Jan. 2018, doi: https://doi.org/10.1016/j.ensm.2017.05.013.

[20] A. Barai, K. Uddin, W. D. Widanage, A. McGordon, and P. Jennings, "A STUDY OF THE INFLUENCE OF MEASUREMENT TIMESCALE ON INTERNAL RESISTANCE CHARACTERISATION METHODOLOGIES FOR LITHIUM-ION CELLS," *Sci Rep*, vol. 8, no. 1, p. 21, Jan. 2018, doi: https://doi.org/10.1038/s41598-017-18424-5.

[21] Xinfan Lin *et al.*, "ONLINE PARAMETERIZATION OF LUMPED THERMAL DYNAMICS IN CYLINDRICAL LITHIUM ION BATTERIES FOR CORE TEMPERATURE ESTIMATION AND HEALTH MONITORING," *IEEE Transactions on Control Systems Technology*, vol. 21, no. 5, pp. 1745–1755, Sep. 2013, doi: https://doi.org/10.1109/TCST.2012.2217143.

[22] N. Kumaresan and A. Rammohan, "EVALUATING THE IMPACT OF AMBIENT TEMPERATURE ON ENERGY CONSUMPTION RATE OF ELECTRIC TWO-WHEELER USING REAL-WORLD DRIVING DATA," *Heliyon*, vol. 10, no. 23, p. e40803, Dec. 2024, doi: https://doi.org/10.1016/j.heliyon.2024.e40803.

[23] J. Bao, Y. Mao, Y. Zhang, H. Xu, Y. Jiang, and Y. Yang, "CRITICAL REVIEW OF TEMPERATURE PREDICTION FOR LITHIUM-ION BATTERIES IN ELECTRIC VEHICLES," *Batteries*, vol. 10, no. 12, p. 421, Nov. 2024, doi: https://doi.org/10.3390/batteries10120421.

[24] S. Kumar Laha, P. Kumar Sadhu, A. Ganguly, and A. Kumar Naskar, "A COMPARATIVE STUDY ON THERMAL PERFORMANCE OF A 3-D MODEL BASED SOLAR PHOTOVOLTAIC PANEL THROUGH FINITE ELEMENT ANALYSIS," *Ain Shams Engineering Journal*, vol. 13, no. 2, p. 101533, Mar. 2022, doi: https://doi.org/10.1016/j.asej.2021.06.019.

[25] G. Sordi *et al.*, "DEGRADATION OF LITHIUM-ION BATTERIES UNDER AUTOMOTIVE-LIKE CONDITIONS: P2D MODEL-BASED UNDERSTANDING AND EX-SITU VALIDATION," *eTransportation*, vol. 24, p. 100410, May 2025, doi: https://doi.org/10.1016/j.etran.2025.100410.

[26] P. Dini, A. Colicelli, and S. Saponara, "REVIEW ON MODELING AND SOC/SOH ESTIMATION OF BATTERIES FOR AUTOMOTIVE APPLICATIONS," *Batteries*, vol. 10, no. 1, p. 34, Jan. 2024, doi: https://doi.org/10.3390/batteries10010034.

[27] S.-J. Park *et al.*, "DEPTH OF DISCHARGE CHARACTERISTICS AND CONTROL STRATEGY TO OPTIMIZE ELECTRIC VEHICLE BATTERY LIFE," *J Energy Storage*, vol. 59, p. 106477, Mar. 2023, doi: https://doi.org/10.1016/j.est.2022.106477.

[28] Z. Zaini, D. M. Harfina, and A. P. Iswar, "REAL-TIME SOC ESTIMATION FOR LI-ION BATTERIES USING KALMAN FILTER BASED ON SBC RASPBERRY-PI," *Andalas Journal of Electrical and Electronic Engineering Technology*, vol. 1, no. 2, pp. 48–57, Dec. 2021, doi: https://doi.org/10.25077/ajeeet.v1i2.12.

[29] S. Kumar Laha, P. Kumar Sadhu, A. Ganguly, and A. Kumar Naskar, "A COMPARATIVE STUDY ON THERMAL PERFORMANCE OF A 3-D MODEL BASED SOLAR PHOTOVOLTAIC PANEL THROUGH FINITE ELEMENT

ANALYSIS," *Ain Shams Engineering Journal*, vol. 13, no. 2, p. 101533, Mar. 2022, doi: https://doi.org/10.1016/j.asej.2021.06.019.

[30] R. A. Thokar, N. Gupta, K. R. Niazi, A. Swarnkar, and N. K. Meena, "MULTIOBJECTIVE NESTED OPTIMIZATION FRAMEWORK FOR SIMULTANEOUS INTEGRATION OF MULTIPLE PHOTOVOLTAIC AND BATTERY ENERGY STORAGE SYSTEMS IN DISTRIBUTION NETWORKS," *J Energy Storage*, vol. 35, p. 102263, Mar. 2021, doi: https://doi.org/10.1016/j.est.2021.102263.